Structural colours in the frond of *Microsorum thailandicum*

Lisa Maria Steiner[1], Yu Ogawa[1,2], Villads Egede Johansen[1], Clive Lundquist[3], Heather Whitney[3], and Silvia Vignolini[1,*]

[1]University of Cambridge, Department of Chemistry, Lensfield Road, Cambridge, CB2 1EW, United Kingdom

[2]Universite Grenoble-Alps, CNRS, CERMAV, 38000 Grenoble, France

[3]University of Bristol, School of Biological Sciences, Tyndall Avenue, Bristol, BS8 1TQ, United Kingdom

[*]Address correspondence to sv319@cam.ac.uk

SUMMARY

Blue and near-ultraviolet structural colours have often been reported in understorey plants living in deep shade. While this intense blue coloration is very catchy to the eye of a human observer, there are cases in which structural colours can be hidden either by the scattered light interacting with pigments or because they are found in unexpected positions in the plants. Here we show that the fronds of *Microsorum thailandicum* produce structural coloration on both the adaxial and abaxial epidermal surface. While cellulose helicoidal structures are responsible for this coloration in both epidermal layers, the reflected colours are consistently different: an intense blue reflection is found in the adaxial epidermis while red-shifted and less intense colours are observed in the abaxial epidermis, possibly suggesting photo-adaptation of the plant to the light environment. By comparing the optical properties of the fern with its anatomy we computed the theoretical reflection accounting for the presence of disorder in the cellulose helicoidal architecture.

Keywords: Structural colour, Plant cell wall, Cellulose helicoidal architecture, *Microsorum thailandicum*, Circular polarisation, Iridescence

1 Background

Structural colours are extremely widespread in nature[1–4]. They do not derive from pigments, but rely on constructive interference of light scattered from nanostructures, with dimensions of the order of the wavelength of visible radiation, 400 - 700 nm[1]. Often, structural colouration can be more intense than colouration by pigments, and can be dependent on the angle of observation. This effect of the reflected wavelength being angle-dependent is called iridescence[3,5]. From flowers[6,7] to fruits[8–10] to leaves[11,12], such brilliant colorations are observed in several plant tissues with different biological functions[13,14], and using several morphologies[1,15]. A common architecture to produce structural colour that is found in several plant tissues consists of cellulose microfibrils assembled into helicoidal architectures in the cell wall[16]. The inherent birefringence of cellulose microfibrils and

their chiral spatial organisation provide a circularly polarised light reflection in a range of wavelengths which are determined by the dimensionality (referred to as pitch) of the helicoid[17]. In more detail, these helicoidal architectures are composed of different layers or pseudolayers of cellulose microfibrils oriented parallel to each other. These layers are stacked up, with a small rotation angle between them. After every 180° rotation, the microfibrils have the same orientation. The distance between two equally orientated layers is defined as the pitch p, and it is related to the reflection maximum λ via $\lambda = 2 \cdot n \cdot p$, where n is the average refractive index n of the medium.

Colour-generating cellulose-based structures are found in the cell wall of many different plant tissues like leaves and fruits[2,18,19], and similar architectures made of chitin have been found in beetles[16,20–22]. In plants, they have been observed via TEM imaging in the juvenile fronds of the fern *Danaea nodosa*[12], via spectroscopy and electron microscopy in the leaves of the Malaysian rain forest understory plants *Lindsaea lucida* and *Diplazium tomentosum*[23], and in the leaves of the tropical rainforest understorey sedge *Mapania caudata*[11]. In fruits, helicoidal cellulose microfibrils architectures have been described in the secondary cell wall of the pericarp of the monocot *Pollia condensata*[8], and in the secondary cell wall of the endocarp of the dicot *Margaritaria nobilis*[9].

However, in leaves, these helicoidal structures have so far only been observed in the adaxial epidermal cell walls and their colour is prevalently in the blue and near UV spectral region. Here, we studied the optical properties and anatomy of *Microsorum thailandicum*, a member of the *Microsorum punctatum* complex of the large fern genus *Microsorum*[24–26]. *M. thailandicum* was described as iridescent by Boonkerd and Nooteboom[24], but the origin of the structural colour was still unclear. In our investigation, we observed that both the adaxial and abaxial epidermal cells contain helicoidal cell walls reflecting blue and green-to-red circularly polarised light, respectively. Finally, by performing electron microscopy and (micro-)spectrophotometry on the same area, we quantitatively correlated the measured reflectivity with the anatomy of the structures, providing an understanding on how the structural disorder affects the optical properties of the fern.

2 Methods

2.1 Plants

Plants were either grown in an office environment or in a growth cabinet set to 25 °C and lowest light option (approx. 2000 lux illuminance) during the day, for 16 hours, and 20 °C and darkness during the night (Panasonic Versatile Environment Test Chamber MLR-352-PE, Panasonic Healthcare Co., Ltd., Japan). They were watered from below once a week and misted daily.

2.2 Photography

Photos of the fern and its fronds were taken with a Nikon D3200 camera (18-55 VR II kit, AF-S DX Nikkor 18-55 mm f/3.5-5.6G VR II, Nikon, Japan), in macro mode, and automatic focussing, using a tripod. A linear polariser was added to reduce gloss from the cuticle (Hoya CIR-PL slim, Hoya corporation, Japan).

2.3 Optical microscopy

Cross-section of fronds A TEM block was made via high pressure freezing and freeze substitution (subsection 2.4) and sliced into semi-thin cross-sections with a Leica Ultracut E ultramicrotome (Leica microsystem GmbH, Austria). It was stained

with Richardson's stain and observed in transmission microscopy on a Zeiss microscope and 5x objective to investigate the ultrastructure of the frond.

Thickness of fronds The thickness of the same fronds used for the gradient investigation (comparison of reflection intensity between fronds, see subsection 3.3) and integrating sphere measurements (for total transmission and reflection, see supporting material SI) was determined by cutting two thin slices in the same tip, middle and base area with a razor blade. Per cross-section, 6 thicknesses were measured, 3 on each side of the frond. They were measured at equal spacing across the area where the frond surface was horizontal (since spectra were also generally taken from that area), aligned with the shortest distance at this cross-sectional point. Images of freshly cut cross-sections of fronds to obtain their thickness were recorded with a Zeiss stereoscope and processed with ImageJ[27,28], see subsection 3.3 and SI.

2.3.1 Polarised optical microscopy and micro-spectroscopy

Optical microscopy was carried out on a customised Zeiss microscope equipped with epi-illumination and a 5x, 20x and 50x objective. Different configurations were used. For polarised optical imaging, the sample was illuminated with an unpolarised halogen lamp, and a polariser and a quarter-waveplate were mounted into the collection optical path, and left and right channel configuration was obtained by independent motors. For images of cells, the 20x objective was used. Spectra were collected via a 100 μm optical fibre mounted in confocal configuration to the focal plane of the objective and connected to a spectrometer (AvaSpec-HS2048 spectrophotometer, spectral range 350-800 nm and resolution of 5 nm). Investigation on the single-cell level was achieved with the 50x objective and the 100 μm optical fibre for collecting spectra. In-house software controlling a motorised stage was employed to scan a single cell with high spatial resolution.

Three fronds from one plant were investigated for the statistics of optical response study, to guarantee equivalent growth conditions.

Three fronds from another plant were investigated with respect to the gradient of structural colour observed, and whether both the adaxial and abaxial surface are always both coloured. Three spectra from the tip, the middle and the base of each frond, adaxial and abaxial surface, were taken.

All fronds were imaged while still on the plant, or alternatively the entire frond was cut off and imaged straight away without making any further cuts on it. Generally, upon being cut off and cut into pieces, the fronds will dry out, the coloration decreases and finally disappears within a few hours.

2.4 Electron microscopy

2.4.1 TEM

Sample embedding by high pressure freezing and freeze substitution 3 mm circular frond samples were cut, placed within brass specimen carriers and loaded into a Leica EM ICE high-pressure freezer, followed by immersion in liquid nitrogen and freeze substitution (Leica AFS2, Leica microsystems GmbH, Germany). The frozen samples still in their carriers were placed inside 2 ml capped cryovials with 1 ml of acetone at the surface of a bath of liquid nitrogen to avoid warming of the samples. The tips of the tweezers were similarly cooled before use. Samples were brought up to room temperature over four days after which they were transferred to 100 % ethanol, followed by a resin series (alcohol:medium grade LR White resin ratios of 3:1,

1:1, 1:3 and 100 % LR White resin). The resin was changed daily over four days after which the specimens were placed in gelatin capsules and polymerised in a Fistreem vacuum oven (digital, Fistreem International Limited, UK) at 60 °C and 440 mmHg for 22 hours. TEM blocks produced via high pressure freezing and freeze substitution were only used for ultrastructure investigations by optical microscopy.

Sample embedding by chemical fixation Small pieces of native, hydrated plant tissue were cut and entirely immersed in a buffered fixative solution containing glutaraldehyde (2 wt%) and formaldehyde (2 wt%) for 16 hours at 4 °C. The specimens were then rinsed with deionised water and fixed for 2 hours at 4 °C in a buffered OsO_4 solution. The specimens were rinsed again in deionised water and successively dehydrated in graded ethanol aqueous solutions (30-100 wt%) and then dry acetonitrile. They were incubated for 16 hours in a 50:50 (v/v) mixture of acetonitrile and Quetol 651 epoxy resin, and subsequently immersed in Quetol resin for 2 weeks, allowing the resin infiltrating into the specimens. The specimens were placed in a silicon mould with Quetol resin and cured for 48 hours at 65 °C. Finally, ultrathin sections were prepared using an ultramicrotome (Ultracut UCT, Leica microsystem GmbH, Austria) equipped with a 35° diamond knife (Diatom, USA) and mounted on continuous carbon coated copper grids. The sections were then post-stained with 1 wt% uranyl acetate aqueous solution and Reynolds lead citrate solution. TEM observations were carried out with a Philips CM-200 'Cryo' electron microscope operated at 200 kV (Thermo Fisher Scientific Inc., USA). All TEM imaging was carried out on blocks made via chemical fixation.

2.4.2 Cryo-SEM

Cryogenic scanning electron microscopy (cryo-SEM) observation was performed using a field-emission scanning electron microscope (Verios 460, Thermo-Fisher Scientific Inc., USA) equipped with a cryo-preparation system (PP3010T, Quorum, UK). The frond was cut into a small strip and mounted upright on a specimen holder using a colloidal graphite suspension. The specimen was quench-frozen in liquid ethane and transferred into the cryo-preparation chamber, where it was freeze-fractured, sublimed, and subsequently sputter-coated with platinum. SEM imaging was carried out at an acceleration voltage of 2 kV and a working distance of approx. 4 mm.

Before cryo-SEM, a few mm wide section of the frond was marked of and polarised optical microscopy carried out on it, so that the optical response could be correlated to the same section of the frond that the cryo-SEM measurements are from. This way, the modelling approach is based on the same small area of the frond.

2.4.3 Block-face SEM

A smooth surface of resin embedded specimen was prepared using an ultramicrotome (Ultracut UCT, Leica microsystem GmbH, Austria) for block-face SEM observation. SEM imaging was carried out using a concentric backscatter (CBS) detector on a field emission scanning electron microscope (Quanta 250, Thermo-Fisher Scientific Inc, USA) operated at 4 kV with a working distance of 7 mm.

2.5 Data and spectra processing

Matlab was used for all data and spectra processing.

Spectra were always referenced to a white diffuser (USRS-99-010, Labsphere, USA), except for the ones used for modelling, which were referenced to a silver mirror (PF10-03-P01, Thorlabs, USA). When referencing to a white diffuser, it is not unusual to obtain reflection intensities higher than unity, in the case that the reflection of the sample is strong and more directional than the white diffuser. Referencing to a silver mirror gives an absolute measure of reflectivity, since all incident light is captured within the numerical aperture of the optical fibre. This is the same referencing method as the one assumed for the modelling.

For the gradient analysis, the spectra of three cells at the tip, the middle and the base of each frond were averaged, for both adaxial and abaxial surface, and a high, a medium and a low structurally coloured frond, respectively.

To obtain histograms of the peak maxima, the inbuilt matlab "maxvalue" function was used. To obtain the full width at half maximum (FWHM), we used the matlab function "findpeaks". The distribution of peak positions was then fitted with a Gaussian distribution, and the distribution of peak widths (FWHM) with a log-normal distribution. For obtaining the average spectra, all spectra of the same surface were averaged.

For the analysis of pitches from the cryo-SEM and block-face SEM images, the imageJ greyscale function was used to count layers. Three lines were measured per cell (corresponding to one SEM image), on the left, middle and right, and these values were averaged, to obtain the average and standard deviation (plotted as error bars) per cell.

Finally, individual spectra are plotted for the modelling section, to demonstrate how much heterogeneity and how many different spectral features are found for different cells.

2.6 Modelling

The freely available Python implementation of Berreman 4x4 (Aug 21, 2016 on github[29]) was used for all simulations, using Python 3.6. We tried out different combinations of parameter fitting of twist defects, pitches, and normal and extraordinary refractive indices in order to match the experimental spectra. The total number of half pitches was fixed to 80 to resemble a total cell wall height of approx. 10 to 15 μm. We used the discrete sum of absolute differences between spectrum and simulation of the main peak as the fitting objective (also called the L1 norm). We fitted only to the main peak since we could not reproduce all spectral features using the Berreman model. It is important to keep in mind that this approach influences the results, but if the main peak is caused by a regular part – potentially located in a more complex structure – then we still obtain a reasonable indication of refractive indices. Since the optimisation problem was expected to have many local minima, we tried the different global optimisation algorithms implemented in the Python library SciPy 0.19. We found that basinhopping worked best for this case and gave most consistent results throughout multiple runs. Convergent results were normally observed within a few minutes, and the optimiser was therefore manually terminated. We found that refractive index parameters of $n_o = 1.528 + 0.0075i$ and $n_e = 1.474 + 0.0075i$ gave a peak height and width that most closely fitted the shape of the main peak of the measurements. Since we do not have enough information to predict the dispersion, and it is expected to be low[30], none was assumed. The refractive indices are close to reported parameters for other helicoidal systems[30,31]. In trying to fit to more complex spectral shapes, we did not obtain any better fit (with realistic parameters) that resembled the shape of the recorded spectra.

3 Results

3.1 Optical response of frond

The optical response of the fronds of *M. thailandicum* was studied using a customised microscopy setup which allows to simultaneously image the epidermis of the frond in different polarisation configurations and to collect spectra in the corresponding imaged area.

Figure 1 A shows a photo of the plant, there are several fronds with an intense blue coloration. Figure 1 B and C depict epi-illumation microscope images of the same area of the adaxial epidermis of a blue frond in the left and right circular polarisation channels (LCP and RCP), respectively. The blue colour, corresponding to the position of the cell in the epidermal layer, is visible only in the LCP, but not in the RCP (Figure 1 B and C), indicating the presence of a helicoidal structure in the cell wall of the outer epidermal cell. Interestingly, the abaxial epidermis displays similar properties: a clear LCP reflection but no RCP reflection is observed from the cells in the green and red spectral region, see Figure 1 E and F, even though the abaxial surface appears non-iridescent by naked eye, as seen on the encircled area in Figure 1 D.

The overall coloration is a combination of structural and pigment colour. The main pigment is chlorophyll and reflects in the green. Since most of the structural colour of the abaxial surface is in a similar range, it is not easily visible by eye.

3.2 Anatomy of frond

Due to the interesting optical appearance, the ultrastructure of the frond was investigated to locate and confirm the helicoidal architecture. Figure 2 A depicts an optical transmission image of a semi-thin cross-section of an embedded frond. Both on the adaxial and abaxial surface, the upper or lower epidermis are clearly visible, the cell walls of these cells look thickened, and the epidermis is covered with the cuticle. The mesophyll consists of the palisade tissue towards the adaxial surface, and the spongy mesophyll towards the abaxial surface.

Zooms of the adaxial and abaxial epidermal cells via cryo-SEM are shown in Figure 2 B-C and E-F, respectively. By increasing the magnification, it is possible to observe a thickened cell wall with a layered structure for the outermost layer of cells in the two epidermises. Furthermore, the same thickening with layered structure can also be observed in the surface-facing side of the cell walls of the second epidermal layer, see red boxes (B-C and E-F). Although ice crystal artifacts are visible in the cell (Figure 2 B and E), the ultrastructure of the epidermal cell walls is considered to be preserved during the sample preparation for cryo-SEM measurements. This is because the growth of ice crystals is likely minimal in the observed area as the secondary cell wall is generally less hydrated than other parts of plant cells, and the epidermal cells are located in the outermost layer of the specimen[32]. TEM imaging was used to further investigate these regions, see Figure 2 D and G, where the Bouligand arcs characteristic for the helicoidal arrangement of cellulose microfibrils in the cell wall are observed[22,33].

3.3 Variation between fronds

When looking at a number of plants (Figure 3 A), we noticed that, even though the macroscopic appearance of a single frond is fairly homogeneous, there is a large amount of variation in intensity of structural coloration between different plants, and even between different fronds on the same plant. Whether and how intensely fronds develop structural coloration probably depends

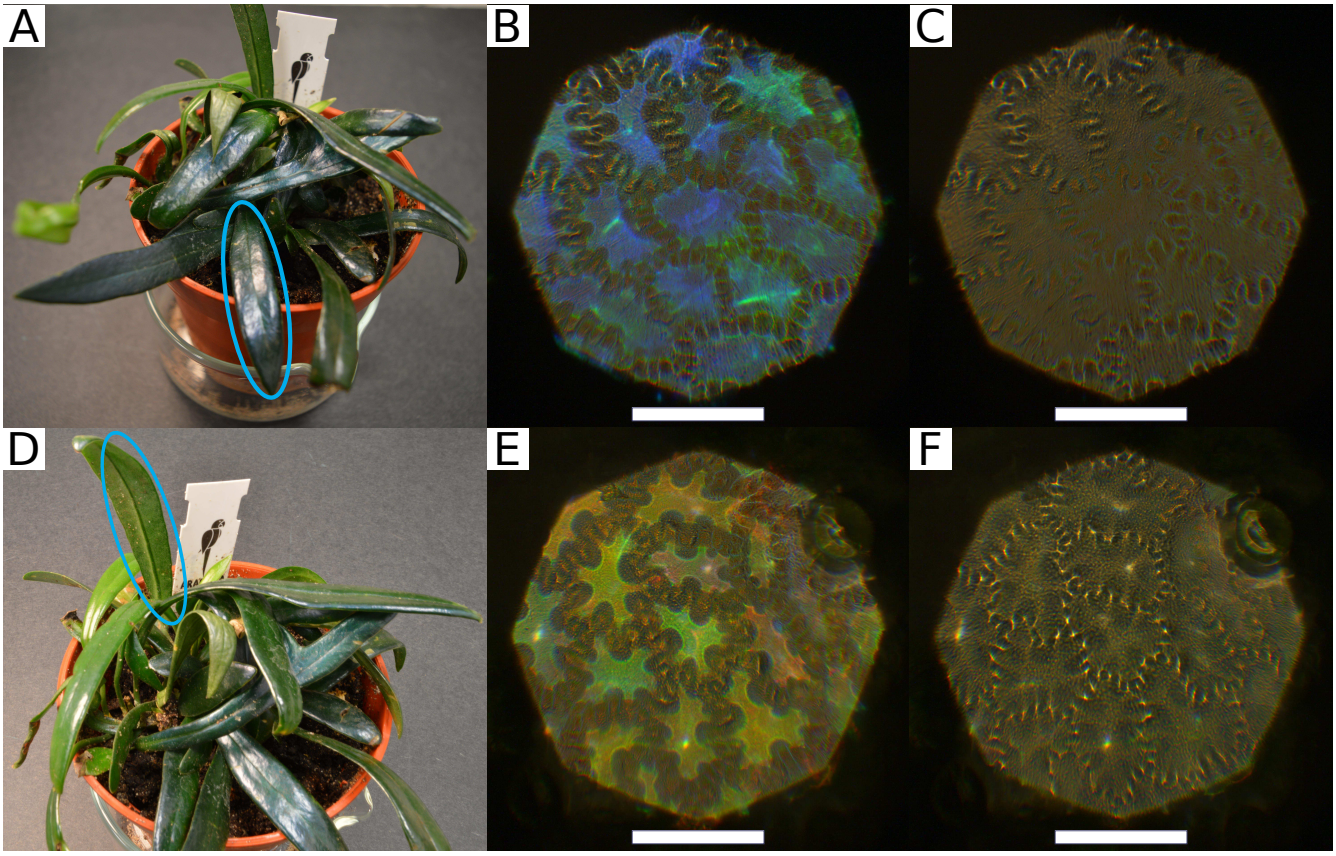

Figure 1. (A) Photo of *M. thailandicum*, adaxial surface encircled in blue was studied. (B,C) Optical micrograph of reflection in left-handed (LCP) and right-handed circular polarised light channel (RCP) of adaxial surface. (D) Photo of *M. thailandicum*, abaxial surface encircled in blue was studied. (E,F) Optical micrograph of reflection in LCP and RCP of abaxial surface. Scale bar is 100 μm.

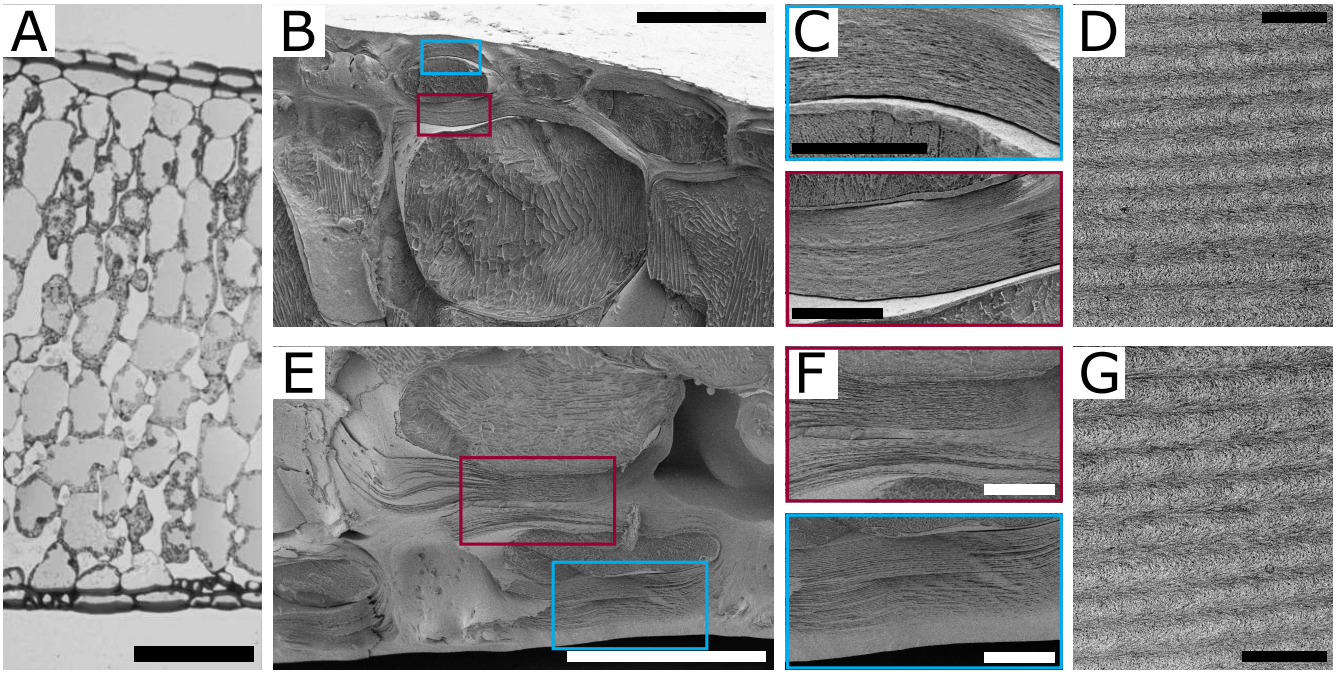

Figure 2. (A) Optical transmission micrograph of semi-thin cross-section of embedded frond. Scale bar is 200 μm. (B,E) Cryo-SEM image of adaxial and abaxial epidermal cells of the frond, respectively. Scale bar is 50 μm. (C,F) Zoom of epidermal cell walls in the blue/red boxes for adaxial and abaxial epidermis, respectively. Scale bar is 10 μm. (D,G) TEM images of adaxial and abaxial cell wall, respectively, showing the Bouligand arcs characteristic for the helicoidal arrangement of cellulose microfibrils. Scale bar is 500 nm.

on a variety of factors, like temperature, light and humidity, which we were not able to fully control over a long enough period of time. To investigate this variation, we studied the intensity and spectral variation of the structural colour in representative fronds from the same plant. The fronds were chosen to have one frond show very intense blue structural colouration on the adaxial surface, one that almost did not show any, and one in between the two extremes. To account for the age of the frond, we collected fronds with comparable stiffness, length and thickness. In more detail, the collected fronds had a thickness of (0.92 ± 0.20) mm for the intensely structurally coloured one, the medium one of (1.00 ± 0.20) mm, and the low coloured one (1.07 ± 0.27) mm.

In particular, we investigated the gradient of structural colour observed, and whether both the adaxial and abaxial surface are always both coloured with the same intensity, see Figure 3 B. As visible in the photograph, the spectra of the most intensely coloured frond showed the highest intensity, the medium coloured frond medium intensity, and the low coloured frond the least intensity of reflection. This trend was observed for both the adaxial and the abaxial surface and structural colouration for both epidermises correlate in intensity, see Figure 3 C-E.

Additionally, integrating sphere measurements of areas of a few millimetre from very strongly and very low structurally coloured fronds were also performed to estimate the total transmission through and reflection of the fronds and the adaxial and abaxial epidermis separately, see SI.

3.4 Variation of the optical response within the same frond

Additionally to the variation of macroscopic appearance of the fronds, variation between the individual cells on each frond is revealed by optical microscopy, see Figure 1 B and E. To characterise this variation, we statistically analysed the optical response of 100 cells of the adaxial surface from the strongly structurally coloured frond shown in Figure 1 A, and 74 cells of the abaxial surface from the strongly structurally coloured frond shown in Figure 1 D. Firstly, the maximum of each LCP reflection was determined for both adaxial and abaxial epidermal cells, and these values were plotted in a histogram, shown in Figure 4 A and D, respectively . The distribution of the maximum reflection wavelength of the peaks is well approximated with a Gaussian distribution, while the distribution of the full width half maximum (FWHM) of the peaks shown in Figure 4 B and E is approximated with a log-normal distribution.

Interestingly, the variation of reflected colours is much narrower for the adaxial surface than for the abaxial surface. For the adaxial surface, all reflection maxima are found between 400-550 nm. The Gaussian distribution gives a mean value of 460 nm, and a standard deviation of $\pm$ 26 nm. This corresponds very closely with the averaged spectrum of all 100 cells, which has a maximum reflection at 461 nm, see the supplementary material (SI). Furthermore, the log-normal fitting of the FWHM histogram yields the values 18.2 nm and 1.4 nm for the mean μ and for σ, giving a standard deviation of $\pm$ 6.7 nm. On the other hand, the reflection of the abaxial epidermis varies much more, all the reflection maxima are found between 400-650 nm, so almost over the entire visible spectrum. When sorting the reflection maxima into a histogram, the approximated Gaussian distribution yields a mean value of 524 nm and a standard deviation of $\pm$ 56 nm. Correspondingly, the shape of the average abaxial reflection spectrum is very wide, and the reflection maximum lies at 511 nm, see SI. Moreover, μ, σ and the standard deviation for the log-normal distribution of peak widths are 21.5, 1.7 and $\pm$ 13.2 nm, respectively, also showing

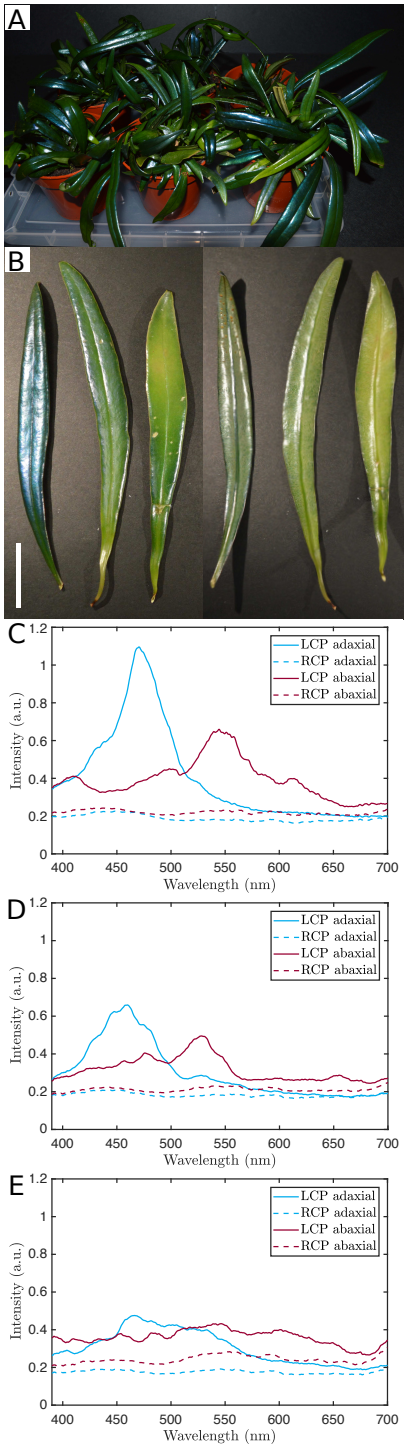

Figure 3. (A) Photo of a variety of specimens. (B) Photo of the adaxial (left) and abaxial (right) surface of three fronds showing high, medium and low structural coloration, from left to right. Scale bar is 2 cm. (C-E) Average reflection spectrum in LCP and RCP of frond, adaxial and abaxial surface: (C) Spectra of the most intensely structurally coloured frond. (D) Spectra of the medium structurally coloured frond. (E) Spectra of the low structurally coloured frond. All spectra are averaged from measurements of nine cells each across the frond.

greater variation than for the adaxial epidermis.

In order to compare these observations to the anatomy of the fronds, we investigated the helicoidal architecture on an individual cell level by electron microscopy. Representative block-face SEM images of the adaxial and abaxial outermost thickened epidermal cell wall used to measure the pitch p are shown in the SI. The pitch p is the height of the helicoidal axis within which the cellulose microfibrils complete a 180° rotation.

The pitch p lies between 150 to 220 nm for the adaxial outermost thickened epidermal cell wall, with most values between 160 and 200 nm, with the standard deviation within each cell below $\pm$ 22 nm, typically below $\pm$ 10 nm, see Figure 4 C (from 24 cells). For the abaxial outermost thickened epidermal cell wall, the pitch p is spread out over a much bigger range, between 120 to 290 nm with most values between 150 and 250 nm, and the standard deviation within each cell is bigger as well, up to $\pm$ 42 nm (from 25 cells), as depicted in Figure 4 F.

The average refractive index n of the medium can be approximated to 1.50, by considering that the typical value of the refractive index for pure crystalline cellulose is 1.55[17], and an average value of 1.45 from the other cell wall components, namely cellulose microfibrils with disordered surface, hemicellulose, lignin, water, small amounts of protein, etc.[34].

Even if the calculated reflection maxima from the pitch data are higher for both adaxial and abaxial cell walls, which is unusual since one may expect shrinkage of structures during the chemical TEM sample processing[35,36], we observed the same trends for both surfaces, using both techniques (cryo-SEM and block-face SEM). We can account for this discrepancy by considering that we are overestimating the pitch by approximately 10%. We believe that the main reason that leads to the measurement of a larger pitch, both with cryo-SEM and block-face SEM, is due to the not perfectly perpendicular cuts with respect to the direction of the helicoidal axis and due to the not perfectly perpendicular measurement direction when processing the images. If the measurement direction is perfectly aligned with the helicoidal axis, the value of the pitch is correct, but any deviation from perfect alignment will always lead to an overestimation of the pitch[37]. While utmost care was taken during measurements and during image processing in imageJ, contributions from this issue cannot be fully excluded, also since the axis of the cell and therefore the helicoids is different from cell to cell and can also change slightly within the cell.

3.5 Variation within single cell

To investigate the disorder in the distribution of the pitch, a single cell of the adaxial epidermis was scanned with larger spatial resolution. Figure 5 A and B report the statistical analysis of the measured reflection spectra (22 in total) as processed in the same way as in subsection 3.4 and in the SI, reporting the reflection maxima in a histogram and the average of all spectra. The average of all 22 spectra of this cell gives a maximum of 506 nm, again corresponding closely with the histogram. Furthermore, all the obtained reflection spectra fall well within the range observed for the previous measurement of 100 adaxial cells across a frond. This means that the variation is the same on a frond, between different cells, as it is within a single cell.

3.6 Modelling the optical response

Next, a very small area of a frond was marked off and subjected both to polarised optical microscopy and then cryo-SEM analyses. A representative optical micrograph of the LCP is shown in Figure 5 D, and example spectra from that area are shown

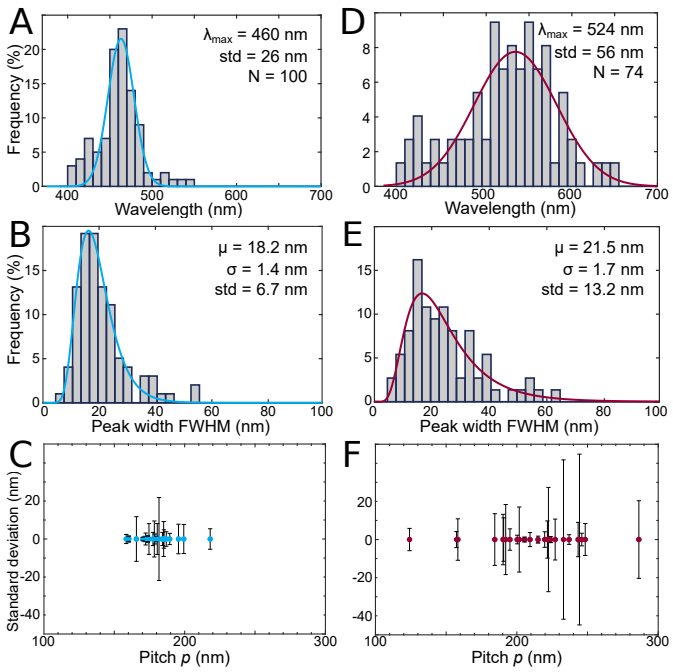

Figure 4. (A-C) Adaxial surface. (A) Distribution of peak wavelengths from structurally coloured cells of frond. (B) Distribution of peak widths as determined by finding the full width at half maximum (FWHM). (C) Distribution of pitches *p* and their standard deviation measured from the layering visible in the uppermost helicoidal cell wall measured from block-face SEM and cryo-SEM images. (D-F) Abaxial surface. Same as for adaxial surface.

in Figure 5 F, while a cryo-SEM image of the layered cell wall of the same area is shown in Figure 5 E. The variation of the pitch p measured from this frond area was then utilised to model the optical response (Figure 5 G).

We modelled the circularly polarised spectral reflection using an open source Python implementation of Berreman's 4x4 matrix method that simulates stratified (layered) anisotropic media[29,38]. This is the most common approach for simulating helicoidally arranged cellulose microfibrils[30]. In Figure 5 G, an ideal helicoidal arrangement of cellulose microfibrils with 40 half pitches of 159.9 nm and refractive indices of $n_o = 1.528 + 0.0075i$ and $n_e = 1.474 + 0.0075i$ was simulated. The figure shows that the main reflection peak position, height and width can be roughly captured, but also that the recorded spectra are much more complex. This is probably due to significant deviations in the helicoidal twist of the cellulose layers from an ideal helicoidal structure (twist defects, varying pitch, etc.) and other geometrical artifacts (curvature of cells, non-planar cellulose layers, etc.). To obtain more information on the arrangement of the cellulose stack, we furthermore tried to use the classifications proposed by Carter et al. for a non-ideal helicoidal reflector in beetles. The best matching classification is 'Spectra with diminishing oscillations', but such spectra are not well described by a few local defects or pitch changes, as described in their supplementary information[39]. Furthermore, looking at individual spectra from several cells (Figure 5 F), we also found that no single classification fitted them all. We therefore conclude that the spectral features indicate a large degree of disorder distributed throughout the cell wall and are not localised to a few defect sites or abrupt pitch changes. This inference corresponds well with the observations made from electron microscopy imaging, see Figure 5 E for an example.

4 Discussion and conclusions

4.1 Colour variation and plant cell wall biosynthesis

Our systematic statistical investigations allow us to conclude that, despite the variation in the reflection response from different fronds in the plant, the reflection maxima of the adaxial epidermis are much narrower with less variation between cells and within cells, compared to the abaxial epidermis. These observations have interesting implications for the biosynthesis of the adaxial versus the abaxial epidermal cell walls. For the abaxial cells, there is much more variation between the different cells, and the range of reflected colours is larger, hence the biosynthesis of the plant cell wall is presumably less orderly regulated than for the adaxial surface. Furthermore, when the reflection wavelength lies at the green or red end of the visible spectrum, it means that the cellulose microfibrils in the helicoidal cell wall architecture have to be spaced further apart than when reflecting in the blue range. We do not know what exactly is used as a spacer between the layers of parallel cellulose microfibrils, but there are at least three different options: *(i) hemicellulose and lignin content.* We think it is most likely that hemicellulose or lignin or both act as a spacer between the cellulose microfibrils. This would mean that in green and red cells, more material, like hemicellulose or lignin is deposited. Quantifying the hemicellulose and lignin content (ideally at a single cell level, but at least for adaxial and abaxial epidermis separately) could give some insights on whether they act as a spacer, in which case their biosynthetic pathways should be investigated further. *(ii) rotation angle.* Another option is that the rotation angle between the cellulose microfibrils is smaller in the abaxial epidermal cell walls. In this case, more layers of cellulose microfibrils would be layered up and would thus increase the pitch, resulting in a shift of reflection to longer wavelengths. If there is a smaller rotation angle between cellulose microfibrils, a higher cellulose content in the abaxial epidermis could be observed. To investigate

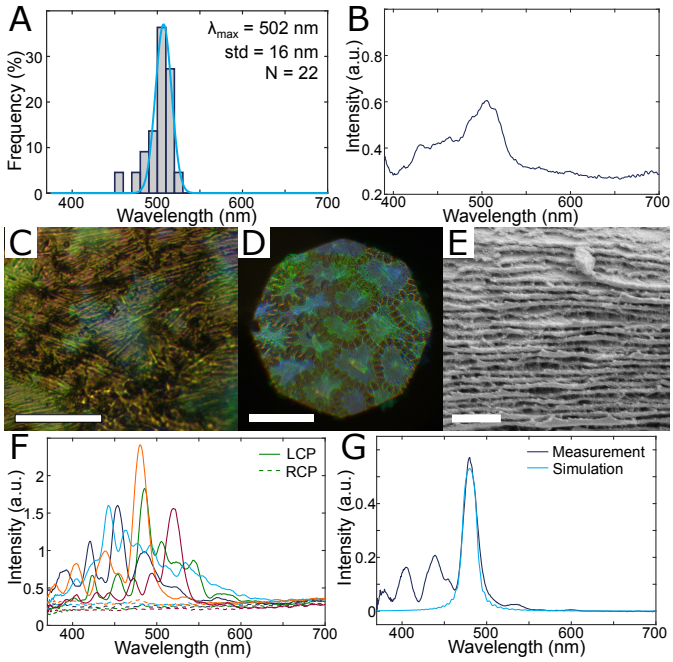

Figure 5. (A) Reflection maxima distribution of single cell. (B) Average spectrum of all 22 LCP spectra from single cell. (C) Optical micrograph of reflection in LCP of single cell of adaxial surface. Scale bar is 20 μm. (D) Optical micrograph of reflection in LCP of adaxial surface, specific part of frond for cryo-SEM. Scale bar is 100 μm. (E) Cryo-SEM micrograph zoom of the helicoidal layering, adaxial surface. Scale bar is 1 μm. (F) Individual reflection spectra in LCP and RCP of 5 cells of a specific part of frond taken for cryo-SEM, adaxial. (G) Measurement taken from a single cell and simulation based on the Berreman 4x4 method (referenced to silver mirror).

this hypothesis, the cellulose content should be investigated for the two epidermises separately. *(iii) water content.* The third option is a difference in water content. The abaxial epidermis does seem more hydrated than the adaxial when preparing TEM specimens, and dehydration does affect the structural colouration of the fronds, making higher water content in the abaxial cell walls an option.

4.2 Influence of disorder on optical response

The model adopted so far to systematically analyse the optical response by helicoidal structures does not encompass all factors contributing to the spectral response. By trying to fit our spectra to the model developed to take into account defects and irregularities in spectra of helicoidal beetle cuticles[39], we were not able to reproduce all the measured spectral features. Therefore, we conclude that a few discrete defect sites do not dominate the reflection spectrum of the plant cell walls. Rather, we expect the reflection to be caused by a more complex and distributed disorder in the cell walls. Looking at spectra from several cells, we also found that no single classification from Carter et al. fitted them all, suggesting that the spectral features indicate a large degree of disorder distributed throughout the cell wall and not localised to a few defect sites or abrupt pitch changes. This conclusion is also supported by our EM imaging, where a lot of small irregularities in the layering can be observed. Furthermore, in our statistical analysis of the variation of reflections on the same frond, we found that the peak widths (FWHM) follow a log-normal distribution, rather than a Gaussian. This hints to the concept that many small defects are found increasing the peak width, and they add up in a logarithmic way.

4.3 Photosynthesis and light harvesting

We speculate that the transmitted light through the adaxial epidermis and mesophyll (including chlorophyll) could then be reflected back into the mesophyll by the abaxial epidermis. So while the mainly blue reflection of the adaxial epidermis could protect the frond from photo-damage in high light conditions, the abaxial epidermis could increase light harvesting in low light conditions, by reflecting parts of the light back into the mesophyll, that would have otherwise been transmitted and lost for photosynthesis. However, investigating this hypothesis experimentally has proved difficult for a number of reasons: *(i) separating the different layers.* Unfortunately it is not possible to remove either of the epidermal layers without damaging the mesophyll. Ideally, we would have measured total transmission through the native frond, and then removed the abaxial epidermis and measured transmission through the adaxial epidermis plus mesophyll. This issue could be circumnavigated by just removing the respective other epidermis, taking spectra thereof and then subtracting them from the spectra of the native frond, but there are additional complications. Even though it is possible to remove either epidermis intact and carefully scrape off remaining mesophyll tissue with a razor blade, even after rinsing, there is always a small amount of chlorophyll left on the epidermis, which is impossible to remove fully without destroying the epidermis, and which is impossible to quantify. This small amount of chlorophyll will always influence measurements in a non-controllable way. *(ii) different amounts of chloroplasts.* Fronds will have different amounts of chlorophyll, and possibly varying ratios of the different types like chlorophyll a and b[40,41]. *(iii) different thicknesses of fronds.* We tried to only pick mature fronds of similar length for analysis to keep results comparable (younger fronds are less stiff and still more flexible), but the plants grow really slowly, and the fronds possibly thicken with age. *(iv) curvature of fronds.* The curvature of fronds varies considerably, and with it the surface

area which is horizontal. This surface property will especially influence reflection properties, unless it is possible to decrease the spot size enough, in which case a large amount of measurements is necessary to obtain meaningful statistics. While the issue of the curvature of fronds *(iv)* could be circumvented by investing a large amount of working hours, tackling the issues of different amounts of chloroplasts *(ii)* and the different thicknesses of fronds *(iii)* are more challenging. Carrying out the integrating sphere measurements requires separating the three layers, and the mesophyll is always destroyed in the process. Hence, the thickness and chlorophyll content could not be determined on the same area of frond either way. Again, carrying out these analyses on a large amount of fronds to obtain meaningful statistics to then relate to any part of frond might be an option.

From our transmission data of the native fronds, we observed that there is very little transmission for most part of the visible spectrum, except for a small spectral area peaking at 550 nm, approximately from 510 to 590 nm. We found this interesting, since the area more or less coincides with the main reflection range of the abaxial epidermis. At the same time, however, there is also an absorption minimum for chlorophyll in this range[40,41], suggesting that there possibly is no optical function of the abaxial reflection.

4.4 Conclusions

In conclusion, we observed that the cell walls of *Microsorum thailandicum* produce structural coloration on both the adaxial and abaxial epidermal surface by a helicoidal architecture of cellulose microfibrils. Whilst there is a large variation in the optical response of the fronds, we find significant trends in the response of the adaxial and abaxial epidermis: the adaxial cell walls cause a much more well-defined reflection than the abaxial cell walls. While the biosynthesis of the plant cell wall and the biological significance of the differences between adaxial and abaxial epidermis are still far from being understood, we speculate that there might be a function in such an optical response, and suggest that there is still a lot to do to understand the strategies that plants use to manage light transport in their tissues.

Supplementary information

Competing interest

We have no competing interests.

Author contributions

LMS, HW, SV designed research, LMS, YO, VEJ, CL, SV performed research, LMS, YO, VEJ, SV analysed data, LMS, SV led the writing of the manuscript, YO, VEJ, CL, HW contributed to discussions. LMS planned experiments, performed optical microscopy and photography, analysed and processed data. YO performed electron microscopy. VEJ performed simulations, automated data acquisition, data processing and data analysis. LMS, SV performed integrating sphere measurements.

Acknowledgements

We thank Bonan Zhu and Gen Kamita for development of software for hyperspectral imaging of the single cell. YO thanks the NanoBio-ICMG platform (FR 2607) for granting access to the electron microscopy facility.

Funding

This work was supported by the European Research Council [ERC-2014-STG H2020 639088], the BBSRC David Phillips Fellowship [BB/K014617/1], the EPSRC [EP/N016920/1], and the European Commission, Marie Curie Fellowship [LODIS 701455].

References

1. Johansen, V. E., Onelli, O. D., Steiner, L. M. & Vignolini, S. Photonics in Nature: From Order to Disorder. In Gorb, S. N. & Gorb, E. V. (eds.) *Functional Surfaces in Biology III*, vol. 10, 53–89 (Springer International Publishing, Cham, 2017). URL http://link.springer.com/10.1007/978-3-319-74144-4_3.

2. Lee, D. W. *Nature's Palette: The Science of Plant Color* (University of Chicago Press, 2007).

3. Vukusic, P. & Sambles, J. R. Photonic structures in biology. *Nature* **424**, 852 (2003).

4. Parker, A. R. 515 million years of structural colour. *Journal of Optics A: Pure and Applied Optics* **2**, R15–R28 (2000). URL http://stacks.iop.org/1464-4258/2/i=6/a=201.

5. Kinoshita, S. *Structural colors in the realm of nature* (World Scientific, 2008).

6. Whitney, H. M. *et al.* Floral Iridescence, Produced by Diffractive Optics, Acts As a Cue for Animal Pollinators. *Science* **323**, 130–133 (2009). URL http://science.sciencemag.org/content/323/5910/130. DOI 10.1126/science.1166256.

7. Moyroud, E. *et al.* Disorder in convergent floral nanostructures enhances signalling to bees. *Nature* **550**, 469–474 (2017). URL http://www.nature.com/doifinder/10.1038/nature24285. DOI 10.1038/nature24285.

8. Vignolini, S. *et al.* Pointillist structural color in Pollia fruit. *Proceedings of the National Academy of Sciences* **109**, 15712–15715 (2012).

9. Vignolini, S. *et al.* Structural colour from helicoidal cell-wall architecture in fruits of *Margaritaria nobilis*. *Journal of The Royal Society Interface* **13**, 20160645 (2016). URL http://rsif.royalsocietypublishing.org/lookup/doi/10.1098/rsif.2016.0645. DOI 10.1098/rsif.2016.0645.

10. Lee, D. W. Ultrastructural basis and function of iridescent blue colour of fruits in Elaeocarpus. *Letters to Nature* **349**, 260–261 (1991).

11. Strout, G. *et al.* Silica nanoparticles aid in structural leaf coloration in the Malaysian tropical rainforest understorey herb Mapania caudata. *Annals of Botany* **112**, 1141–1148 (2013). URL https://academic.oup.com/aob/article-lookup/doi/10.1093/aob/mct172. DOI 10.1093/aob/mct172.

12. Graham, R. M., Lee, D. W. & Norstog, K. Physical and Ultrastructural Basis of Blue Leaf Iridescence in Two Neotropical Ferns. *American Journal of Botany* **80**, 198 (1993). URL http://doi.wiley.com/10.1002/j.1537-2197.1993.tb13789.x. DOI 10.2307/2445040.

13. Thomas, K. R., Kolle, M., Whitney, H. M., Glover, B. J. & Steiner, U. Function of blue iridescence in tropical understorey plants. *Journal of The Royal Society Interface* **7**, 1699–1707 (2010). URL http://rsif.royalsocietypublishing.org/cgi/doi/10.1098/rsif.2010.0201. DOI 10.1098/rsif.2010.0201.

14. Jacobs, M. *et al.* Photonic multilayer structure of Begonia chloroplasts enhances photosynthetic efficiency. *Nature Plants* **2** (2016). URL http://www.nature.com/articles/nplants2016162. DOI 10.1038/nplants.2016.162.

15. Vignolini, S., Moyroud, E., Glover, B. J. & Steiner, U. Analysing photonic structures in plants. *Journal of The Royal Society Interface* **10**, 20130394–20130394 (2013). URL http://rsif.royalsocietypublishing.org/cgi/doi/10.1098/rsif.2013.0394. DOI 10.1098/rsif.2013.0394.

16. Wilts, B. D., Whitney, H. M., Glover, B. J., Steiner, U. & Vignolini, S. Natural Helicoidal Structures: Morphology, Self-assembly and Optical Properties. *Materials Today: Proceedings* **1**, 177–185 (2014). URL http://linkinghub.elsevier.com/retrieve/pii/S2214785314000224. DOI 10.1016/j.matpr.2014.09.021.

17. Wilts, B. D., Dumanli, A. G., Middleton, R., Vukusic, P. & Vignolini, S. Invited Article: Chiral optics of helicoidal cellulose nanocrystal films. *APL Photonics* **2**, 0408011–0408017 (2017). URL http://aip.scitation.org/doi/10.1063/1.4978387. DOI 10.1063/1.4978387.

18. Neville, A. C. & Levy, S. The helicoidal concept in plant cell wall ultrastructure and morphogenesis. In *Biochemistry of plant cell walls*, no. 28 in Society for Experimental Biology (Brett C.T., Hillmann J.R., 1985).

19. Roland, J. C., Reis, D., Vian, B., Satiat-Jeunemaitre, B. & Mosiniak, M. Morphogenesis of plant cell walls at the supramolecular level: internal geometry and versatility of helicoidal expression. *Protoplasma* **140**, 75–91 (1987).

20. Jewell, S. A., Vukusic, P. & Roberts, N. W. Circularly polarized colour reflection from helicoidal structures in the beetle *Plusiotis boucardi*. *New Journal of Physics* **9**, 99–99 (2007). URL http://stacks.iop.org/1367-2630/9/i=4/a=099?key=crossref.0d36b979612bb0d89564fe342c13c913. DOI 10.1088/1367-2630/9/4/099.

21. Sharma, V., Crne, M., Park, J. O. & Srinivasarao, M. Structural origin of circularly polarized iridescence in jeweled beetles. *science* **325**, 449–451 (2009).

22. Middleton, R., Steiner, U. & Vignolini, S. Chapter 17 Bio-mimetic Structural Colour using Biopolymers. In *Bio-inspired Polymers*, 555–585 (The Royal Society of Chemistry, 2017). URL http://dx.doi.org/10.1039/9781782626664-00555.

23. Gould, K. S. & Lee, D. W. Physical and Ultrastructural Basis of Blue Leaf Iridescence in Four Malaysian Understory Plants. *American Journal of Botany* **83**, 45 (1996). URL http://doi.wiley.com/10.1002/j.1537-2197.1996.tb13872.x. DOI 10.2307/2445952.

24. Boonkerd, T. & Nooteboom, H. P. A new species of Microsorum (Polypodiaceae) from Thailand. *Blumea* **46**, 581–583 (2001).

25. Petchsri, S. *et al.* Phenetic study of the Microsorum punctatum complex (Polypodiaceae). *ScienceAsia* **38**, 1–12 (2012).

26. Kreier, H.-P., Zhang, X.-C., Muth, H. & Schneider, H. The microsoroid ferns: Inferring the relationships of a highly diverse lineage of Paleotropical epiphytic ferns (Polypodiaceae, Polypodiopsida). *Molecular Phylogenetics and Evolution* **48**, 1155–1167 (2008). URL http://linkinghub.elsevier.com/retrieve/pii/S1055790308002182. DOI 10.1016/j.ympev.2008.05.001.

27. Schneider, C. A., Rasband, W. S. & Eliceiri, K. W. NIH Image to ImageJ: 25 years of image analysis. *Nature methods* **9**, 671 (2012).

28. ImageJ. URL https://imagej.net/Welcome.

29. https://github.com/Berreman4x4/Berreman4x4 (2018).

30. Dumanli, A. G. *et al.* Digital Color in Cellulose Nanocrystal Films. *ACS Applied Materials & Interfaces* **6**, 12302–12306 (2014). URL http://pubs.acs.org/doi/10.1021/am501995e. DOI 10.1021/am501995e.

31. Sultanova, N., Kasarova, S. & Nikolov, I. Dispersion properties of optical polymers. *Acta Physica Polonica-Series A General Physics* **116**, 585 (2009).

32. Cosgrove, D. J. & Jarvis, M. C. Comparative structure and biomechanics of plant primary and secondary cell walls. *Frontiers in Plant Science* **3** (2012). URL http://journal.frontiersin.org/article/10.3389/fpls.2012.00204/abstract. DOI 10.3389/fpls.2012.00204.

33. Bouligand, Y. Twisted fibrous arrangements in biological materials and cholesteric mesophases. *Tissue and Cell* **4**, 189–217 (1972). URL http://www.sciencedirect.com/science/article/pii/S0040816672800429. DOI https://doi.org/10.1016/S0040-8166(72)80042-9.

34. Buchanan, B. B., Gruissem, W. & Jones, R. L. *Biochemistry & molecular biology of plants* (American Soc. of Plant Physiologists, Rockville, Md, 2009), 7. reprint. edn.

35. Denef, J.-F., Cordier, A. C., Mesquita, M. & Haumont, S. The influence of fixation procedure, embedding medium and section thickness on morphometric data in thyroid gland. *Histochemistry and Cell Biology* **63**, 163–171 (1979).

36. Mollenhauer, H. H. Artifacts caused by dehydration and epoxy embedding in transmission electron microscopy. *Microscopy research and technique* **26**, 496–512 (1993).

37. Frka-Petesic, B., Kamita, G., Guidetti, G. & Vignolini, S. The angular optical response of cellulose nanocrystal films explained by the structural distortions of the arrested suspension upon drying. *In preparation.* (2018).

38. Berreman, D. W. Optics in stratified and anisotropic media: 4$\times$ 4-matrix formulation. *Journal of the Optical Society of America* **62**, 502–510 (1972).

39. Carter, I. E., Weir, K., McCall, M. W. & Parker, A. R. Variation in the circularly polarized light reflection of *Lomaptera* (Scarabaeidae) beetles. *Journal of The Royal Society Interface* **13**, 20160015 (2016). URL http://rsif.royalsocietypublishing.org/lookup/doi/10.1098/rsif.2016.0015. DOI 10.1098/rsif.2016.0015.

447 **40.** Cordón, G. B. & Lagorio, M. G. Optical properties of the adaxial and abaxial faces of leaves. Chlorophyll fluorescence,
448 absorption and scattering coefficients. *Photochemical & Photobiological Sciences* **6**, 873 (2007). URL http://xlink.
449 rsc.org/?DOI=b617685b. DOI 10.1039/b617685b.

450 **41.** Wolf, F. T. Chlorophylls A and B in the Pteridophytes. *Bulletin of the Torrey Botanical Club* **85**, 1 (1958). URL
451 https://www.jstor.org/stable/2482444?origin=crossref. DOI 10.2307/2482444.